A New Electron Acceptor with End-Extended Conjugation for High Performance Polymer Solar Cells

Jingnan Wu,[a,d,e] Qi Liu,[a] Long Ye,[c] Xia Guo, [a,b] Qunping Fan,[a] Junfang Lv, [a] Maojie Zhang*,[a] Wai-Yeung Wong*[b]*

[a] Laboratory of Advanced Optoelectronic Materials, College of Chemistry, Chemical Engineering and Materials Science, Soochow University, Suzhou 215123, China.

E-mail: guoxia@suda.edu.cn; mjzhang@suda.edu.cn

[b] Department of Applied Biology and Chemical Technology and Research Institute for Smart Energy, The Hong Kong Polytechnic University, Hung Hom, Hong Kong, China.

E-mail: wai-yeung.wong@polyu.edu.hk

[c] Department of Physics and ORaCEL, North Carolina State University, Raleigh, NC27695, USA.

[d]Department of Chemistry and Bioscience, Aalborg University, DK-9220 Aalborg, Denmark.

[e]Department of Chemistry and Chemical Engineering, Chalmers University of Technology, Göteborg, SE-412 96, Sweden.

TABLE OF CONTENTS

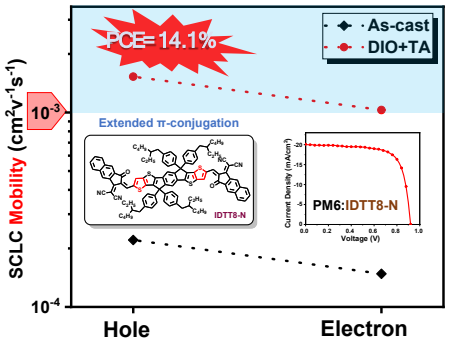

ABSTRACT: To develop high efficiency polymer solar cells (PSCs), the acceptors in bulk-heterojunction (BHJ) blend are supposed to possess complementary absorption bands in the near-infrared region and suitable energy level to be well-matched with the donors. In this work, a new small molecular acceptor (SMA) named IDTT8-N based on indacenodithienothiophene (IDTT) core was designed and synthesized. Compared with the counterpart molecule IDTN with indacenodithiophene (IDT) core, IDTT8-N with the extended π-conjugation length of IDT core not only exhibits a red-shift of ca. 35 nm in optical absorption, but also has little change on its lowest unoccupied molecular orbital (LUMO) energy level. Therefore, PSCs based on PM6:IDTT8-N exhibit superior short-circuit current density (J_{sc}) and high open-circuit voltage (V_{oc}). Moreover, apart from the strong face-on molecular stacking, distinct end-group π-π stacking of IDTT8-N can be observed in the blends, facilitating the charge transport. Therefore, the optimized PM6:IDTT8-N based devices exhibit dramatically high and balanced electron mobility (μ_e) and hole mobility (μ_h), whose magnitudes are over 10^{-3} cm^2 V^{-1} s^{-1}. Consequently, an extraordinary PCE of 14.1% with a relatively high J_{sc} of 20.98 mA cm^{-2} and a V_{oc} of 0.94 V was recorded. To our knowledge, it is the new record among PSCs with SMA based on the 2-(3-oxocyclopentylidene)malononitrile (INCN) as end-groups. These results indicate that extending the π-conjugation length of the fused ring core of SMA is an efficient method to both enhance the absorption and the molecular interaction of acceptor as well as the photovoltaic performance of PSCs.

KEYWORDs: solar energy; polymer solar cells; small molecule acceptor; indacenodithienothiophene (IDTT) core; 2-(3-oxocyclopentylidene)malononitrile end group;

INTRODUCTION

With some unique characteristics such as low-cost, light-weight and flexibility, polymer solar cell (PSC) is a promising renewable energy technology.[1-3] Compared to fullerene derivatives as the acceptors, which show low absorption, limited tuning of

energy levels and poor stability, non-fullerene acceptors (NFAs) show great tunability in the absorption spectrum and electronic energy level as well as excellent thermal stability, providing a wide range of new opportunities in this field.[4-7] Owing to the advanced achievement in synthetic methods, materials design strategies and device engineering, the power conversion efficiency (PCE) of the state-of-the-art single junction bulk heterojunction (BHJ) PSC now exceeds 18%.[8-15] To satisfy the demands of complementary absorption spectra, well-matched energy levels and suitable aggregation behavior of NFAs, rational modifications of the molecular structures of NFAs are as significant as device optimization to make more breakthroughs in PSCs.

In general, most reported high-performance small molecular acceptors (SMAs) are based on the acceptor-donor-acceptor (A-D-A) structure composed of an electron-rich core and electron-withdrawing functional group.[16-24] Each component of the A-D-A structure can be independently modified, which offers great synthetic flexibility by modulating the aromatic core, either in the side chains or terminal groups, and thus readily tunable optical, electronic and morphological properties can be achieved. For instance, Zhan et al. increased the number of aromatic fused-rings from five to seven to enhance the molar extinction coefficient and intramolecular charge transfer (ICT) effect with the two end groups, thus leading to improvement of the short-circuit current density (J_{sc}) in PSCs.[25] Side-chain engineering plays an important role with greatly altered crystallinity, alignment and morphology,[8, 25-29] like the change of SMA from Y6[7] to N3[22] or BTP-eC9.[21] Moreover, the end groups can be modified by various strategies, especially for electronegative fluorine substituent.[30-32] To date, most of the top-performing acceptors, such as IT-4F[27] and Y6-type acceptors, contain fluorine atoms.

Recently, the terminal group named 2-(3-oxocyclopentylidene)malononitrile (INCN) with π-conjugation extension by fusing two phenyl rings, which exhibits high electron mobility and stronger molecular aggregation in the corresponding SMA, has attracted considerable attention for designing highly efficient PSC materials.[33-38] However, the problems of IC-N-based acceptors, such as IDTN reported by Hou and

co-workers, show limited visible light absorption region with a moderate bandgap about 1.59 eV, leading to inferior J_{sc} in the resulting PSCs.[38] To solve this issue, some works extend the length of the electron-rich core by introducing the alkylthiophene π-bridges to strengthened the ICT effect and yielded an increased J_{sc} but sacrificed the open-circuit voltage (V_{oc}).[34] Therefore, it is still a challenging task for broadening the optical absorption of IC-N-based acceptors while maintaining high V_{oc} for the device performance.

Herein, we designed and synthesized a novel electron acceptor named IDTT8-N based on a bulky seven-ring fused indacenodithienothiophene (IDTT) core and end-capped with IC-N groups. The extended conjugation length of fused ring core can enhance the electron donating property, which is beneficial to molecular packing and enables the BHJ layers to effectively utilize solar photons in the range of 600-900 nm with a narrow optical bandgap of 1.53 eV. Meanwhile, the steric effect of 4-(2-ethylhexyl)phenyl substituents can suppress the aggregation of the large coplanar π-system to ensure solubility for solution processing and appropriate aggregation in the blend films with conjugated polymer donor. Notably, in comparison with IDTN, IDTT8-N shows a red-shift of ca. 35 nm in the optical absorption and a negligible ca. 10 meV downshift of the LUMO level, but the resulting device based on PM6[34]:IDTT8-N yields a high V_{oc} of 0.94 V (0.946 V for reported PM6:IDTN-based device).[33] Most importantly, after device optimizations, the IDTT8-N-based device exhibits the dramatically high μ_e and μ_h of over 10^{-3} cm^2 V^{-1} s^{-1}, owing to the strong face-on molecular stacking and distinct π-π stacking of the end group of IDTT8-N. Consequently, we achieved an extraordinary PCE of 14.1% with a relatively high J_{sc} of 20.98 mA/cm^2 and an FF of 0.72. To our best knowledge, this result is so far the best efficiency reported in the literature for PSCs based on acceptor materials with INCN as the end-group.[33-38]

RESULTS AND DISCUSSION

Synthesis and characterization

The synthetic routes and molecular structure of IDTT8-N are shown in **Scheme S1** and **Figure 1a**, respectively. Details of the synthesis and their characterizations are given in the Experimental Section in the Supporting Information. The chemical structures of the intermediates and IDTT8-N were confirmed by Proton and carbon nuclear magnetic resonance (^{1}H NMR, ^{13}C NMR) and Matrix-Assisted Laser Desorption/Ionization Time of Flight Mass Spectrometry (MALDI-TOF MS). IDTT8-N shows good solubility in common organic solvents, such as chloroform (CF), chlorobenzene (CB) and 1,2-dichlorobenzene (DCB) at room temperature. The thermal stability of IDTT8-N was determined by using thermogravimetric analysis, as shown in **Figure S1** in the Supporting Information. The decomposition temperature (T_d, 5% weight-loss) of IDTT8-N is 359 °C, indicating that it possesses splendid thermal stability.

Optical and Electrochemical Properties

The solution and thin-film absorption spectra of IDTT8-N were recorded on a UV–vis spectrophotometer and the data are presented in **Figure 1b**. In solution, IDTT8-N exhibits a strong absorption in the region of 550-780 nm with a high maximum extinction coefficient of 2.2 × 10^5 M^{-1} cm^{-1} at 712 nm (**Figure S2,** Supporting Information). From solution to thin film, the maximum absorption peak of IDTT8-N shows a remarkable red-shift of ca. 28 nm, indicating the compact molecular stacking in the solid state of IDTT8-N. According to the absorption onsets, the optical bandgap of IDTT8-N is 1.53 eV with a decrease of 0.06 eV in comparison with that of IDTN (1.59 eV). The high-performance wide bandgap polymer, PM6, was chosen as the donor and it shows a strong absorption in the region of 400-650 nm, which complements well with IDTT8-N.

Electrochemical properties of IDTT8-N were investigated by cyclic voltammetry (CV) measurement[40] **(Figure 1c**). The onset potentials of oxidation (E_{ox}) and

reduction (E_{red}) for IDTT8-N are 0.95 and -0.73 V versus Fc/Fc$^+$, respectively. As shown in **Figure 1d,** the highest occupied molecular orbital (HOMO) and LUMO energy levels of IDTT8-N were calculated to be −5.67 and −3.98 eV, respectively, which exhibits a higher HOMO and a similar LUMO relative to IDTN (E_{HOMO} = –5.77 eV; E_{LUMO} = –3.97 eV). Hence, the ΔE_{HOMO} and energy loss (E_{loss}) that is estimated from the lowest optical bandgap of the donor and acceptor components, based on PM6:IDTT8-N pair and PM6:IDTN pair are 0.17/0.59 eV and 0.27/0.64 eV, respectively. The results indicate that, after the rational chemical modification, we can get an appropriate energy level of IDTT8-N, which is beneficial for achieving a lower energy loss in the PSCs.

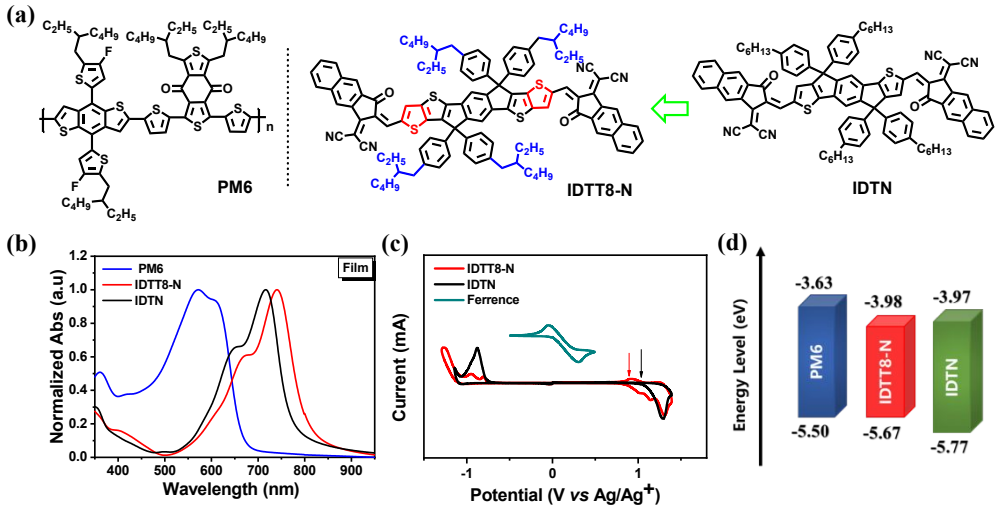

Figure. 1. (a) Chemical structures of PM6, IDTT8-N and IDTN. (b) Normalized UV-vis-NIR absorption spectra of PM6, IDTT8-N and IDTN thin films. (c) Cyclic voltammograms of IDTT8-N and IDTN films on a glassy carbon electrode measured in a 0.1 mol/L Bu_4NPF_6 acetonitrile solution at a scan rate of 50 mV/s. (d) Energy level diagrams for PM6, IDTT8-N and IDTN.

Photovoltaic properties

The PSCs with a conventional structure of ITO/PEDOT:PSS/PM6:IDTT8-N/PFN-Br/Al were fabricated to evaluate the photovoltaic performance of IDTT8-N. The photovoltaic parameters, current density versus voltage (*J-V*) curves and histograms of PCEs of the PM6:IDTT8-N based PSCs

are collected in **Table 1** and **Figure 2**, respectively. The PM6:IDTT8-N device without post treatment affords a PCE of 11.2% with a V_{oc} of 0.97 V, a J_{sc} of 18.3 mA cm^{-2}, and an FF of 0.63. Solvent additive and thermal annealing (TA) treatments were chosen to control the nanoscale morphology of the active layer and enhance the device performance. 1,8-Diiodooctane (DIO) was selected to be the most suitable solvent additive for this system. For the contents of DIO (DIO/CF, v/v) from 0.25% to 0.75%, the active layer processed by annealing at 100 ^{o}C for 5 min exhibited PCEs over 13% with significantly enhanced J_{sc} of 19.5-20.9 mA/cm^2 and FF of 0.72-0.73, and an optimal PCE of 14.1% was obtained with 0.25% DIO (**Figure S3-S5** and **Table S1-S3** in Supporting Information). Moreover, the optimal PSCs also showed a relatively low E_{loss} of *ca.* 0.59 eV, which is less than the PM6:IDTN-based device of 0.64 eV, corresponding to the variation in energy level.

As shown in **Figure 2b**, the external quantum efficiency (EQE) is obviously enhanced for the solar cells with solvent additive and TA treatment. When 0.25% DIO and annealing treatment at 100 °C for 5 min were used to enhance the photovoltaic performance, the quantum efficiency of the device was significantly increased in the wavelength range of 400-860 nm, and a maximum EQE value of 0.78 at 680 nm was recorded. The corresponding integral current densities for PM6:IDTT8-N based PSC with and without optimal treatment are 17.2 and 20.1 mA/cm^2, respectively, which match well with the J_{sc} obtained from the *J-V* measurements with the errors both within 5%.

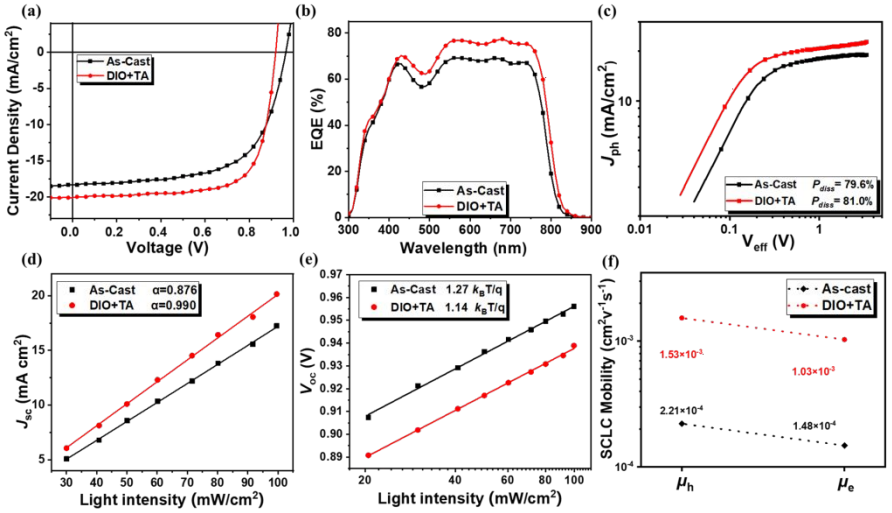

Figure 2. (a) Current density-voltage characteristics of the PSCs under AM 1.5G illumination at 100 mW/cm^2. (b) EQE spectra of the corresponding PSCs; (c) J_{ph}-V_{eff} characteristics, (d) Current density and (e) V_{oc} versus light intensity based on PM6: IDTT8-N (1:1). (f) Hole and electron mobilities of the PSCs with or without post-treatment.

Table 1. Photovoltaic performance of the PSCs based on PM6:IDTT8-N (1:1, w/w) under the illumination of AM 1.5 G at 100 mW/cm^2.

Device	V_{oc} [V]	J_{sc} [mA/cm^2]	Cal. J_{sc}[d)] [mA/cm^2]	FF	PCE [%]
PM6:IDTT8-N[a)]	0.97	18.3	17.2	0.63	11.2 (10.9±0.2)[e)]
PM6:IDTT8-N[b)]	0.94	20.9	20.1	0.72	14.1 (13.8±0.3)[e)]
PM6:IDTN[c)]	0.946	16.58	16.02	0.78	12.2 (12.0±0.2)

a) As-cast. b) 0.25% DIO+100℃. c) Ref 33. d) The integral J_{sc} from the EQE curves. e) The average values and standard deviations of the device parameters based on 20 devices are shown in brackets.

Exciton Dissociation and Charge Recombination

To investigate the combined influence of solvent additive DIO and TA treatment on the exciton dissociation and charge collection process, we measured the exciton dissociation probabilities P(E,T) that can be estimated using the J_{ph}/J_{sat} ratio in the device.[41] **Figure 2c** shows the photocurrent density (J_{ph}) against the effective voltage (V_{eff}) curves. J_{ph} is defined as $J_L - J_D$, where J_L and J_D are the current densities under

illumination and in the dark, respectively. V_{eff} is defined as $V_0 - V_a$, where V_0 is the voltage at which the photocurrent is zero and V_a is the applied voltage. For the PM6:IDTT8-N solar cells, J_{ph} reaches saturation (J_{sat}) at large V_{eff} ($V_{eff} \geq 2$ V), suggesting that all of the photogenerated excitons are dissociated into free carriers and collected by the electrodes. Under maximal power output conditions (P_{max}), the ratios were 79.6% for the as-cast device and 81.0% for the optimal device, respectively. The improved P(E, T) implied that the PSC device leads to more efficient exciton dissociation and charge collection efficiency after solvent additive and TA treatment, which may contribute to the increase J_{sc} and FF in the PSCs.

The photoluminescence (PL) spectra of PM6 or IDTT8-N neat film and the blend film as cast or after TA treatment were investigated to explore the exciton dissociation in the blend films. As shown in **Figure S6** in the Supporting Information, the selected excitation wavelength for PM6 is 600 nm while that for IDTT8-N is 700 nm according to their maximum absorptions. For the donor PM6, its emission spectrum is located in the range of 630-840 nm when excited at a wavelength of 600 nm. For PM6:IDTT8-N blend films with or without post-treatment, the quenched efficiencies are 93% and 90%, indicating effective electron transfer from PM6 to IDTT8-N for the optimal device. Upon exciting the acceptor IDTT8-N at a wavelength of 700 nm, the PL spectrum of the IDTT8-N neat film appears within 720-1000 nm. For the blend films, the PL spectral intensities are quenched by 95% for as cast device and 96% for the optimal device. Overall, the PM6:IDTT8-N based device with optimal condition exhibits the most efficient charge separation in the active layer.

Charge-carrier recombination in the blend films was examined by measuring the dependence of J_{sc} and V_{oc} under different light intensities. As shown in **Figure 2d**, the relationship between J_{sc} and P_{light} which is described by $J_{sc} \propto (P_{light})^S$, where S is the exponential factor and the slope (S value) close to 1 indicates weak bimolecular recombination in the device.[42] The devices showed an S value of 0.876 for the as-cast device, while the S value of 0.990 was obtained for the optimized device, which indicates that bimolecular recombination was efficiently suppressed in the optimized

one. The higher exciton dissociation efficiency and weaker bimolecular recombination in the devices with optimal treatment were well consistent with the higher J_{sc} and PCE values. **Figure 2e** shows the relationship between V_{oc} and P_{light} and the slope of V_{oc} versus lg(P_{light}) can be used to estimate the degree of trap-assisted bimolecular or recombination. Generally, the trap-assisted recombination is dominant when the slope is equal to 2 k_BT/q, meanwhile, the slope of k_BT/q suggests that the bimolecular recombination is dominant.[43] In this work, the devices based on PM6:IDTT8-N showed a slope of 1.27 kT_B/q for the as-cast device and 1.14 k_BT/q for the optimal device, respectively, indicating that the bimolecular recombination is dominant in the devices. After solvent additive and TA treatment, the trap-assisted recombination in device gets reduced and higher FF can be obtained.

Charge transport properties

The charge transport properties of the PM6:IDTT8-N film with optimal treatment and as-cast were evaluated for hole-only devices ITO/PEDOT:PSS/PM6:IDTT8-N/MoO_3/Al and electron-only devices ITO/ZnO-NP/PM6:IDTT8-N/PFN-Br/Al by the space-charge limited current (SCLC) method[44] (**Figure S7** in Supporting Information). As shown in **Figure 2f**, the electron mobility (μ_e) and hole mobility (μ_h) for the as-cast film were calculated to be 2.21 × 10^{-4} and 1.48 × 10^{-4} cm^{-2} V^{-1} s^{-1}, respectively. It is important to note that both μ_e and μ_h increased greatly after solvent additive and TA treatment, which were calculated to be 1.53 × 10^{-3} and 1.03 × 10^{-3} cm^{-2} V^{-1} s^{-1}, respectively. The higher and balanced charge mobilities lead to less charge recombination, thus improving the J_{sc} and FF.

Morphology Characterization

Grazing incidence wide-angle X-ray scattering (GIWAXS) was employed to investigate the molecular stacking information of IDTT8-N neat film and PM6:IDTT8-N blend films.[45] The 2D-GIWAXS patterns and corresponding scattering profiles in the in-plane (IP) and out-of-plane (OOP) directions are presented in **Figure**

3a-b. As indicated in **Figure S8**, the pure IDTT8-N film exhibits a very strong (010) π-π staking peak in the OOP direction, located at 1.73 $Å^{-1}$ with a d-spacing of 3.63 Å, indicating that IDTT8-N exhibits strong crystallinity and face-on molecular orientation. Meanwhile, two distinct lamellar diffraction peaks in the IP direction can be observed, located at 0.29 $Å^{-1}$and 0.33 $Å^{-1}$ with d-spacing of 21.7 Å and 19.0 Å, respectively, which can be attributed to the co-existence of lamellar stacking and end-group π-π staking.[46]

According to the 1D profiles in the IP direction, the (100) peaks of PM6:IDTT8-N system before any treatment is mainly located at 0.33 $Å^{-1}$. After being treated with 0.25% DIO and annealing, two distinct and sharp lamellar diffraction peaks are located at 0.28 $Å^{-1}$ and 0.34 $Å^{-1}$, respectively. To have more details of the morphological change, we performed the Gaussian fitting analysis for the (100) peaks of the 1D cuts in the IP direction. We tried to divide the (100) peaks for as-cast PM6:IDTT8-N films into two peaks according to the IDTT8-N pure films. As indicated from **Figure S9** and **Table S5,** 0.25% DIO and annealing treatment can both facilitate the lamellar stacking and end-group π-π staking of IDTT8-N, in accordance with the higher charge transport as mentioned above. In the OOP direction, (010) peak for as-cast PM6:IDTT8-N is located at 1.79 $Å^{-1}$ with the d-spacing of 3.51 Å while that for the blend films with 0.25% DIO and annealing treatment is located at 1.80 $Å^{-1}$ with the d-spacing of 3.49 Å. We calculated the coherence length (CL) of π-π staking, which was calculated from the full width at half maximum (FWHM) of OOP using Scherrer equation.[47] PM6:IDTT8-N film with 0.25% DIO and annealing treatment exhibits a larger CL of 24 nm than the as-cast film of 18 nm. Promoted by the DIO additive and annealing treatment, the higher crystallinity and favorable face-on molecular orientation are beneficial to the charge transfer, thereby inducing superior J_{sc} and FF.

The variation in length scale of phase separation and domain purity of PM6:IDTT8-N was investigated by resonant soft X-ray scattering (R-SoXS).[48] The 1D scattering profiles shown in **Figure 3c** are Lorentz corrected and thickness

normalized, and the optimum photon energy was selected to be 283.6 eV. The as-cast PM6:IDTT8-N blend film showed a discernable broad hump at q~0.14 nm^{-1}, corresponding to the domain length scales (long periods) of ≈45 nm. The processing condition does not affect the long period much, as after optimization by DIO additive and annealing treatment, the broad hump was located at q~0.14 nm^{-1}, corresponding to the long periods of ≈42 nm, and the smaller long period leads to a higher J_{sc}. Also, 0.25% DIO and annealing treatment improves the relative phase purity of the blend film from 0.66 to 1, contributing to the great enhancement in FF.

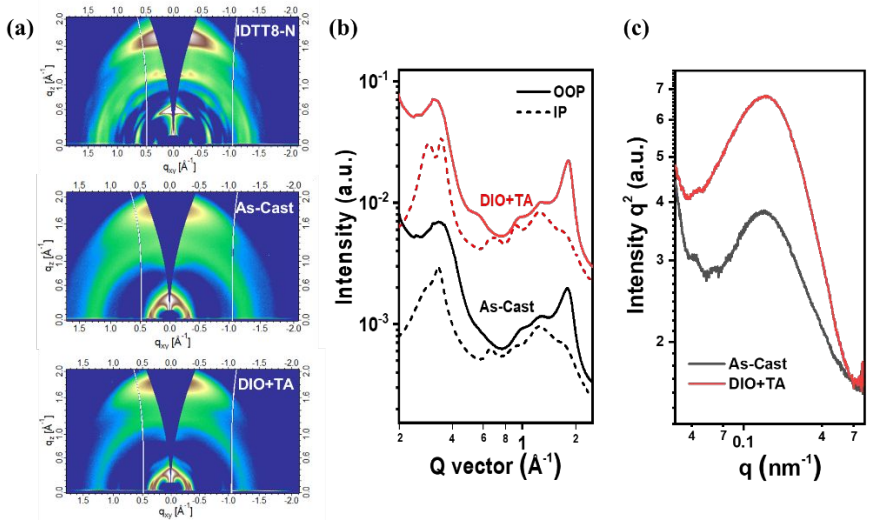

Figure 3. (a) 2D-GIWAXS patterns of pure IDTT8-N film and PM6:IDTT8-N blend films without or with 0.25% DIO and annealing treatment. (b) Scattering profiles and (c) R-SoXS profiles for PM6:IDTT8-N blend films without or with 0.25% DIO and annealing treatment.

To clarify the effect of morphology on the photovoltaic performance, the active layers of the optimized devices were studied using atomic force microscopy (AFM) and transmission electron microscopy (TEM) as shown in **Figure 4**. In the AFM height images, the root-mean-square (RMS) roughness of pristine photoactive blends and optimal blend films are 1.46 and 2.42 nm, respectively. As shown in the phase images, there is no obvious phase separation in the PM6:IDTT8-N pristine blend film while the PM6:IDTT8-N optimal blend film shows large aggregations after adding

0.25% DIO with TA treatment that exhibits clear phase separation with nanostructure, which increases the D/A interface and benefits exciton dissociation and contributes to the least charge recombination for the improved J_{sc} and FF in the PSC. Moreover, as demonstrated in the TEM images, both films exhibited distinct interpenetrating networks and similar phase separation. Compared to the pristine blend film, the optimal film showed broader fibrous features, and the fibril width may extend the exciton diffusion length, which is beneficial for exciton dissociation and charge transport as well as reduces the trap-assisted recombination in the PSC device.

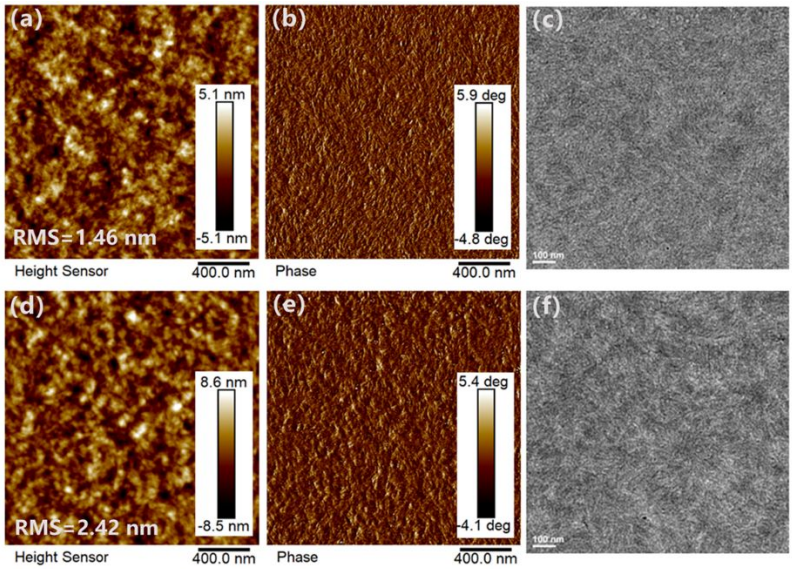

Figure 4. The AFM and TEM images of the PM6:IDTT8-N blend films: (a), (b) and (c) for the blend without as-cast treatment; and (d), (e) and (f) for the blend with 0.25% DIO and TA treatment.

CONCLUSIONS

In conclusion, we designed and synthesized a novel electron acceptor IDTT8-N based on indacenodithieno[3,2-b]thiophene core. Due to the extended π-conjugation length at the core of this molecule, IDTT8-N shows a red-shift in the optical absorption in comparison with the previous molecule IDTN with IDT core. Most importantly, this modification has only little impact on its LUMO energy levels, and thus, PSCs based on PM6:IDTTN-8 maintain relatively high V_{oc}. Besides, after device optimization, the IDTT8-N-based device exhibits the dramatically high μ_e and μ_h,

owing to the distinct end-group π-π stacking and strong face-on molecular stacking. Consequently, we achieved an extraordinary PCE of 14.1%. Our work provides an experimental strategy that underpins the high performance observed for IDTT-based acceptors and has implications for future non-fullerene acceptor design.

SUPPORTING INFORMATION

The Supporting Information is available free of charge on the ACS Publications website.

TGA spectra, absorption spectra and GIWAXS scattering profiles of IDTT8-N, $J-V$ curves and photovoltaic parameters of the PSCs with different contents of DIO, annealing temperature and annealing time of PM6:IDTT8-N (1:1, w/w). PL spectra, charge mobilities and gaussian fitting analysis for GIWAXS plots of related blend films. (PDF)

NOTES

The authors declare no competing financial interest.

ACKNOWLEDGMENTS

This study was supported by National Natural Science Foundation of China (NSFC) (No. 51773142 and 51973146), Jiangsu Provincial Natural Science Foundation (Grant No. BK20190099), the Priority Academic Program Development of Jiangsu Higher Education Institutions, and Collaborative Innovation Center of Suzhou Nano Science Technology. W.-Y. W. thanks the financial support from the Hong Kong Research Grants Council (PolyU 153051/17P and C5037-18G), Research Institute for Smart Energy (CDA2), Hong Kong Polytechnic University (1-ZE1C) and the Endowed Professorship in Energy from Ms Clarea Au (847S).

REFERENCES

1. Lu, L.; Zheng, T.; Wu, Q.; Schneider, A. M.; Zhao, D.; Yu, L., Recent Advances in Bulk Heterojunction Polymer Solar Cells. *Chem. Rev.* **2015,** 115, (23), 12666-12731.

2. Ostroverkhova, O., Organic Optoelectronic Materials: Mechanisms and Applications. *Chem. Rev.* **2016,** 116, (22), 13279-13412.

3. Wang, Y.; Lee, J.; Hou, X.; Labanti, C.; Yan, J.; Mazzolini, E.; Parhar, A.; Nelson, J.; Kim, J. S.; Li, Z., Recent Progress and Challenges toward Highly Stable Nonfullerene Acceptor-Based Organic Solar Cells. *Adv. Energy Mater.* **2020,** 11, (5), 2003002.

4. Jia, B.; Zhan, X., Fused-ring electron acceptors in China. *Sci. China Chem.* **2020,** 63, (9), 1179-1181.

5. Lin, Y.; Wang, J.; Zhang, Z. G.; Bai, H.; Li, Y.; Zhu, D.; Zhan, X., An electron acceptor challenging fullerenes for efficient polymer solar cells. *Adv. Mater.* **2015,** 27, (7), 1170-1174.

6. Wei, Q.; Liu, W.; Leclerc, M.; Yuan, J.; Chen, H.; Zou, Y., A-DA′D-A non-fullerene acceptors for high-performance organic solar cells. *Sci. China Chem.* **2020,** 63, (10), 1352-1366.

7. Yuan, J.; Zhang, Y.; Zhou, L.; Zhang, G.; Yip, H.-L.; Lau, T.-K.; Lu, X.; Zhu, C.; Peng, H.; Johnson, P. A.; Leclerc, M.; Cao, Y.; Ulanski, J.; Li, Y.; Zou, Y., Single-Junction Organic Solar Cell with over 15% Efficiency Using Fused-Ring Acceptor with Electron-Deficient Core. *Joule* **2019,** 3, (4), 1140-1151.

8. Li, C.; Zhou, J.; Song, J.; Xu, J.; Zhang, H.; Zhang, X.; Guo, J.; Zhu, L.; Wei, D.; Han, G.; Min, J.; Zhang, Y.; Xie, Z.; Yi, Y.; Yan, H.; Gao, F.; Liu, F.; Sun, Y., Non-fullerene acceptors with branched side chains and improved molecular packing to exceed 18% efficiency in organic solar cells. *Nature Energy* **2021**, DOI: 10.1038/s41560-021-00820-x.

9. Lin, Y.; Firdaus, Y.; Isikgor, F. H.; Nugraha, M. I.; Yengel, E.; Harrison, G. T.; Hallani, R.; El-Labban, A.; Faber, H.; Ma, C.; Zheng, X.; Subbiah, A.; Howells, C. T.; Bakr, O. M.; McCulloch, I.; Wolf, S. D.; Tsetseris, L.; Anthopoulos, T. D., Self-Assembled Monolayer Enables Hole Transport Layer-Free Organic Solar Cells with 18% Efficiency and Improved Operational Stability. *ACS Energy Lett.* **2020,** 5, (9), 2935-2944.

10. Qin, J.; Zhang, L.; Zuo, C.; Xiao, Z.; Yuan, Y.; Yang, S.; Hao, F.; Cheng, M.; Sun, K.; Bao, Q.; Bin, Z.; Jin, Z.; Ding, L., A chlorinated copolymer donor demonstrates a 18.13% power conversion efficiency. *J. Semiconductors* **2021,** 42, (1), 010501.

11. Wu, J.; Li, G.; Fang, J.; Guo, X.; Zhu, L.; Guo, B.; Wang, Y.; Zhang, G.; Arunagiri, L.; Liu, F.; Yan, H.; Zhang, M.; Li, Y., Random terpolymer based on thiophene-thiazolothiazole unit

enabling efficient non-fullerene organic solar cells. *Nat. Commun.* **2020,** 11, (1), 4612.

12. Xiong, J.; Xu, J.; Jiang, Y.; Xiao, Z.; Bao, Q.; Hao, F.; Feng, Y.; Zhang, B.; Jin, Z.; Ding, L., Fused-ring bislactone building blocks for polymer donors. *Sci. Bull.* **2020,** 65, (21), 1792-1795.

13. Zhan, L.; Li, S.; Xia, X.; Li, Y.; Lu, X.; Zuo, L.; Shi, M.; Chen, H., Layer-by-Layer Processed Ternary Organic Photovoltaics with Efficiency over 18%. *Adv. Mater.* **2021,** 33, (12), 2007231.

14. Zhang, M.; Zhu, L.; Zhou, G.; Hao, T.; Qiu, C.; Zhao, Z.; Hu, Q.; Larson, B. W.; Zhu, H.; Ma, Z.; Tang, Z.; Feng, W.; Zhang, Y.; Russell, T. P.; Liu, F., Single-layered organic photovoltaics with double cascading charge transport pathways: 18% efficiencies. *Nat. Commun.* **2021,** 12, (1), 309.

15. Guo, X.; Fan, Q.; Wu, J.; Li, G.; Peng, Z.; Su, W.; Lin, J.; Hou, L.; Qin, Y.; Ade, H.; Ye, L.; Zhang, M.; Li, Y., Optimized Active Layer Morphologies via Ternary Copolymerization of Polymer Donors for 17.6% Efficiency Organic Solar Cells with Enhanced Fill Factor. *Angew Chem. Int. Ed. Engl.* **2021,** 60, (5), 2322-2329.

16. Cheng, P.; Li, G.; Zhan, X.; Yang, Y., Next-generation organic photovoltaics based on non-fullerene acceptors. *Nat. Photonics* **2018,** 12, (3), 131-142.

17. Hou, J.; Inganas, O.; Friend, R. H.; Gao, F., Organic solar cells based on non-fullerene acceptors. *Nat. Mater.* **2018,** 17, (2), 119-128.

18. Yan, C.; Barlow, S.; Wang, Z.; Yan, H.; Jen, A. K. Y.; Marder, S. R.; Zhan, X., Non-fullerene acceptors for organic solar cells. *Nat. Rev. Mater.* **2018,** 3, (3), 18003.

19. Zhang, J.; Tan, H. S.; Guo, X.; Facchetti, A.; Yan, H., Material insights and challenges for non-fullerene organic solar cells based on small molecular acceptors. *Nat. Energy* **2018,** 3, (9), 720-731.

20. An, N.; Cai, Y.; Wu, H.; Tang, A.; Zhang, K.; Hao, X.; Ma, Z.; Guo, Q.; Ryu, H. S.; Woo, H. Y.; Sun, Y.; Zhou, E., Solution-Processed Organic Solar Cells with High Open-Circuit Voltage of 1.3 V and Low Non-Radiative Voltage Loss of 0.16 V. *Adv. Mater.* **2020,** 32, (39), e2002122.

21. Tang, A.; Song, W.; Xiao, B.; Guo, J.; Min, J.; Ge, Z.; Zhang, J.; Wei, Z.; Zhou, E., Benzotriazole-Based Acceptor and Donors, Coupled with Chlorination, Achieve a High VOC of 1.24 V and an Efficiency of 10.5% in Fullerene-Free Organic Solar Cells. *Chem. Mater.* **2019,** 31, (11),

3941-3947.

22. Wang, X.; Tang, A.; Yang, J.; Du, M.; Li, J.; Li, G.; Guo, Q.; Zhou, E., Tuning the intermolecular interaction of A2-A1-D-A1-A2 type non-fullerene acceptors by substituent engineering for organic solar cells with ultrahigh VOC of ~1.2 V. *Sci. China Chem.* **2020,** 63, (11), 1666-1674.

23. Zhang, X.; Qin, L.; Yu, J.; Li, Y.; Wei, Y.; Liu, X.; Lu, X.; Gao, F.; Huang, H., High-Performance Noncovalently Fused-Ring Electron Acceptors for Organic Solar Cells Enabled by Noncovalent Intramolecular Interactions and End-Group Engineering. *Angew Chem. Int. Ed. Engl.* **2021,** 60, (22), 12475-12481.

24. Ma, Y.; Cai, D.; Wan, S.; Yin, P.; Wang, P.; Lin, W.; Zheng, Q., Control over π-π stacking of heteroheptacene-based nonfullerene acceptors for 16% efficiency polymer solar cells. *Natl. Sci. Rev.* **2020,** 7, (12), 1886-1895.

25. Dai, S.; Zhao, F.; Zhang, Q.; Lau, T. K.; Li, T.; Liu, K.; Ling, Q.; Wang, C.; Lu, X.; You, W.; Zhan, X., Fused Nonacyclic Electron Acceptors for Efficient Polymer Solar Cells. *J. Am. Chem. Soc.* **2017,** 139, (3), 1336-1343.

26. Cui, Y.; Yao, H.; Zhang, J.; Xian, K.; Zhang, T.; Hong, L.; Wang, Y.; Xu, Y.; Ma, K.; An, C.; He, C.; Wei, Z.; Gao, F.; Hou, J., Single-Junction Organic Photovoltaic Cells with Approaching 18% Efficiency. *Adv. Mater.* **2020,** 32, (19), 1908205.

27. Jiang, K.; Wei, Q.; Lai, J. Y. L.; Peng, Z.; Kim, H. K.; Yuan, J.; Ye, L.; Ade, H.; Zou, Y.; Yan, H., Alkyl Chain Tuning of Small Molecule Acceptors for Efficient Organic Solar Cells. *Joule* **2019,** 3, (12), 3020-3033.

28. Zhang, Z.-G.; Li, Y., Side-chain engineering of high-efficiency conjugated polymer photovoltaic materials. *Sci. China Chem.* **2014,** 58, (2), 192-209.

29. Zhu, C.; Meng, L.; Zhang, J.; Qin, S.; Lai, W.; Qiu, B.; Yuan, J.; Wan, Y.; Huang, W.; Li, Y., A Quinoxaline-Based D-A Copolymer Donor Achieving 17.62% Efficiency of Organic Solar Cells. *Adv. Mater.* **2021**, 2100474.

30. Chen, Y.; Bai, F.; Peng, Z.; Zhu, L.; Zhang, J.; Zou, X.; Qin, Y.; Kim, H. K.; Yuan, J.; Ma, L. K.; Zhang, J.; Yu, H.; Chow, P. C. Y.; Huang, F.; Zou, Y.; Ade, H.; Liu, F.; Yan, H., Asymmetric Alkoxy and Alkyl Substitution on Nonfullerene Acceptors Enabling High-Performance Organic Solar Cells. *Adv. Energy Mater.* **2020,** 11, (3), 2003141.

31. Karki, A.; Vollbrecht, J.; Gillett, A. J.; Selter, P.; Lee, J.; Peng, Z.; Schopp, N.; Dixon, A. L.; Schrock, M.; Nádaždy, V.; Schauer, F.; Ade, H.; Chmelka, B. F.; Bazan, G. C.; Friend, R. H.; Nguyen, T. Q., Unifying Charge Generation, Recombination, and Extraction in Low-Offset Non-Fullerene Acceptor Organic Solar Cells. *Adv. Energy Mater.* **2020,** 10, (29), 2001203.

32. Zhao, W.; Li, S.; Yao, H.; Zhang, S.; Zhang, Y.; Yang, B.; Hou, J., Molecular Optimization Enables over 13% Efficiency in Organic Solar Cells. *J. Am. Chem. Soc.* **2017,** 139, (21), 7148-7151.

33. Feng, H.; Qiu, N.; Wang, X.; Wang, Y.; Kan, B.; Wan, X.; Zhang, M.; Xia, A.; Li, C.; Liu, F.; Zhang, H.; Chen, Y., An A-D-A Type Small-Molecule Electron Acceptor with End-Extended Conjugation for High Performance Organic Solar Cells. *Chem. Mater.* **2017,** 29, (18), 7908-7917.

34. Li, R.; Liu, G.; Xiao, M.; Yang, X.; Liu, X.; Wang, Z.; Ying, L.; Huang, F.; Cao, Y., Non-fullerene acceptors based on fused-ring oligomers for efficient polymer solar cells via complementary light-absorption. *J. Mater. Chem. A* **2017,** 5, (45), 23926-23936.

35. Su, N.; Ma, R.; Li, G.; Liu, T.; Feng, L.-W.; Lin, C.; Chen, J.; Song, J.; Xiao, Y.; Qu, J.; Lu, X.; Sangwan, V. K.; Hersam, M. C.; Yan, H.; Facchetti, A.; Marks, T. J., High-Efficiency All-Polymer Solar Cells with Poly-Small-Molecule Acceptors Having π-Extended Units with Broad Near-IR Absorption. *ACS Energy Lett.* **2021,** 6, (2), 728-738.

36. Swick, S. M.; Zhu, W.; Matta, M.; Aldrich, T. J.; Harbuzaru, A.; Lopez Navarrete, J. T.; Ponce Ortiz, R.; Kohlstedt, K. L.; Schatz, G. C.; Facchetti, A.; Melkonyan, F. S.; Marks, T. J., Closely packed, low reorganization energy pi-extended postfullerene acceptors for efficient polymer solar cells. *Proc. Natl. Acad. Sci. USA* **2018,** 115, (36), E8341-E8348.

37. Wang, N.; Zhan, L.; Li, S.; Shi, M.; Lau, T.-K.; Lu, X.; Shikler, R.; Li, C.-Z.; Chen, H., Enhancement of intra- and inter-molecular π-conjugated effects for a non-fullerene acceptor to achieve high-efficiency organic solar cells with an extended photoresponse range and optimized morphology. *Mater. Chem. Front.* **2018,** 2, (11), 2006-2012.

38. Li, S.; Ye, L.; Zhao, W.; Liu, X.; Zhu, J.; Ade, H.; Hou, J., Design of a New Small-Molecule Electron Acceptor Enables Efficient Polymer Solar Cells with High Fill Factor. *Adv. Mater.* **2017,** 29, (46), 1704051.

39. Zhang, M.; Guo, X.; Ma, W.; Ade, H.; Hou, J., A Large-Bandgap Conjugated Polymer for

Versatile Photovoltaic Applications with High Performance. *Adv. Mater.* **2015,** 27, (31), 4655-4660.

40. Guo, B.; Li, W.; Guo, X.; Meng, X.; Ma, W.; Zhang, M.; Li, Y., High Efficiency Nonfullerene Polymer Solar Cells with Thick Active Layer and Large Area. *Adv. Mater.* **2017,** 29, (36), 1702291.

41. Wu, J. L.; Chen, F. C.; Hsiao, Y. S.; Chien, F. C.; Chen, P.; Kuo, C. H.; Huang, M. H.; Hsu, C. S., Surface plasmonic effects of metallic nanoparticles on the performance of polymer bulk heterojunction solar cells. *ACS Nano* **2011,** 5, (2), 959-967.

42. Lenes, M.; Morana, M.; Brabec, C. J.; Blom, P. W. M., Recombination-Limited Photocurrents in Low Bandgap Polymer/Fullerene Solar Cells. *Adv. Funct. Mater.* **2009,** 19, (7), 1106-1111.

43. Koster, L. J. A.; Mihailetchi, V. D.; Ramaker, R.; Blom, P. W. M., Light intensity dependence of open-circuit voltage of polymer:fullerene solar cells. *Appl. Phys. Lett.* **2005,** 86, (12).

44. Proctor, C. M.; Kim, C.; Neher, D.; Nguyen, T.-Q., Nongeminate Recombination and Charge Transport Limitations in Diketopyrrolopyrrole-Based Solution-Processed Small Molecule Solar Cells. *Adv. Funct. Mater.* **2013,** 23, (28), 3584-3594.

45. Zhu, L.; Zhong, W.; Qiu, C.; Lyu, B.; Zhou, Z.; Zhang, M.; Song, J.; Xu, J.; Wang, J.; Ali, J.; Feng, W.; Shi, Z.; Gu, X.; Ying, L.; Zhang, Y.; Liu, F., Aggregation-Induced Multilength Scaled Morphology Enabling 11.76% Efficiency in All-Polymer Solar Cells Using Printing Fabrication. *Adv. Mater.* **2019,** 31, (41), 1902899.

46. Mai, J.; Xiao, Y.; Zhou, G.; Wang, J.; Zhu, J.; Zhao, N.; Zhan, X.; Lu, X., Hidden Structure Ordering Along Backbone of Fused-Ring Electron Acceptors Enhanced by Ternary Bulk Heterojunction. *Adv. Mater.* **2018**, 30, (34), e1802888.

47. Muller-Buschbaum, P., The active layer morphology of organic solar cells probed with grazing incidence scattering techniques. *Adv. Mater.* **2014,** 26, (46), 7692-7709.

48. Gann, E.; Young, A. T.; Collins, B. A.; Yan, H.; Nasiatka, J.; Padmore, H. A.; Ade, H.; Hexemer, A.; Wang, C., Soft x-ray scattering facility at the Advanced Light Source with real-time data processing and analysis. *Rev. Sci. Instrum.* **2012,** 83, (4), 045110.